Dynamics of ordering of Heisenberg spins with torque: Nonconserved case

Jayajit Das* and Madan Rao†
Institute of Mathematical Sciences, Taramani, Madras 600113, India
(Received 26 September 1997)

We study the dynamics of ordering of a nonconserved Heisenberg magnet. The dynamics consists of two parts — an irreversible dissipation into a heat bath and a reversible precession induced by a torque due to the local molecular field. For quenches to zero temperature, we provide convincing arguments, both numerically (Langevin simulation) and analytically (approximate closure scheme due to Mazenko), that the torque is irrelevant at late times. We subject the Mazenko closure scheme to systematic numerical tests. Such an analysis, carried out on a vector order parameter, shows that the closure scheme performs respectably well. For quenches to T_c, we show, to $O(\epsilon^2)$, that the torque is irrelevant at the Wilson-Fisher fixed point. [S1063-651X(98)05105-8]

PACS number(s): 64.60.My, 64.60.Cn, 68.35.Fx

I. INTRODUCTION

Interacting systems such as magnets and binary fluids exhibit an ordered configuration at low temperatures, consisting of coexisting, symmetry broken phases. When cooled rapidly from the disordered phase at high temperatures, such systems take a long time to establish order, primarily because of the slow annealing of the interfaces (defects) separating the competing domains. At late times, the system organizes itself into a self-similar spatial distribution of domains characterized by a single diverging length scale that typically grows algebraically in time $L(t)\sim t^{1/z}$. This spatial distribution of domains is reflected in the scale dependent behavior of the correlation functions.

In the last few years, a fairly detailed picture of the late time behavior of the correlation functions has emerged [1]. The equal-time order parameter correlation function $C(r,t) \equiv\langle \vec{\phi}(r,t)\cdot\vec{\phi}(0,t)\rangle$ is a measure of the spatial distribution of the domains, and at late times is found to behave as $f(r/L(t))$, where $L(t)$ is the distance between defects. The autocorrelation function, $C(0,t_1=0,t_2)\equiv\langle \vec{\phi}(0,0)\cdot\vec{\phi}(0,t_2)\rangle$, is a measure of the memory of the initial configurations, and decays at late times as $L(t_2)^{-\lambda}$. The independent scaling exponents z and λ and the scaling function $f(x)$ characterize the dynamical universality classes at the zero temperature fixed point [1].

The scaling results referred to above have been obtained in systems coupled to a constant temperature heat bath, where the order parameter $\vec{\phi}(r,t)$ undergoes a purely dissipative (irreversible) dynamics. There is no dynamics of the order parameter in the absence of this coupling. In general, however, apart from dissipating into a heat bath, the system may have a Hamiltonian dynamics of its own. Such dynamics can be represented by a generalized Langevin equation [2],

$$\frac{\partial\phi_\alpha(r,t)}{\partial t}=\int_{r',t'}\{\phi_\alpha(r,t),\phi_\beta(r',t')\}\frac{\delta F}{\delta\phi_\beta(r',t')} -\Gamma(-i\nabla)^\mu\frac{\delta F}{\delta\phi_\alpha(r,t)}+\eta_\alpha(r,t), \tag{1}$$

where ϕ_α is an N-component order parameter, F is a coarse-grained free-energy functional, $\{\cdot,\cdot\}$ is the Poisson bracket, and η_α is the noise. The first term on the right hand side is reversible, while the second is the usual dissipative force, with $\mu=2$ or 0 according to whether the order parameter is conserved or not. The noise correlator $\langle\eta_\alpha(r,t)\eta_\beta(r',t')\rangle = 2\Gamma k_B T\delta_{\alpha\beta}(-i\nabla)^\mu\delta(r-r')\delta(t-t')$ is proportional to the temperature T.

As an example let us consider the dynamics of a binary fluid given by the generalized Langevin description Eq. (1). The relative concentration ϕ of a binary fluid is advected by the velocity field $\mathbf{v}=\mathbf{g}/\rho$. The generalized Langevin equation for ϕ involves the reversible $\{\phi,g_\alpha\}\delta F/\delta g_\alpha$, which reduces to the familiar streaming term $\mathbf{v}\cdot\nabla\phi$ [1].

One might classify the dynamics according to the algebraic structure of the Poisson brackets. For instance, the Poisson algebra of the components of the order parameter could be of the form $\{\phi_\alpha,\phi_\beta\}=c$, where c is in general a complex number. A recently studied example is the dynamics of superfluid ordering of a Bose gas [3]. The dynamics is written in terms of a complex boson annihilation field ψ, which obeys the Poisson bracket relation $\{\psi,\psi^*\}=i$. On the other hand, the Poisson algebra of the components of the order parameter could be a Lie algebra $\{\phi_\alpha,\phi_\beta\} = c_{\alpha\beta\gamma}\phi_\gamma$, where $c_{\alpha\beta\gamma}$ are the structure constants. A common example is the dynamics of the local magnetic moments of a Heisenberg magnet. The components of the magnetic moments ϕ_α ($\alpha=1,2,3$) satisfy the Poisson algebra,

$$\{\phi_\alpha(r,t),\phi_\beta(r',t')\}=\Omega_L\epsilon_{\alpha\beta\gamma}\phi_\gamma(r,t)\delta(r-r')\delta(t-t'), \tag{2}$$

where $\epsilon_{\alpha\beta\gamma}$ is the completely antisymmetric tensor in three dimensions and Ω_L is the Larmour frequency.

This paper provides a detailed discussion of the phase ordering dynamics of a nonconserved Heisenberg magnet in

*Electronic address: jayajit@imsc.ernet.in
†Electronic address: madan@imsc.ernet.in

three dimensions. In a future companion paper, we plan to discuss the conserved ordering dynamics. This paper is broken down as follows. After a brief account of the dynamics of the model (Sec. II), we discuss the dynamics of phase ordering following a quench to $T=0$ (Sec. III). A Langevin simulation and an analytical calculation using the approximate closure scheme of Mazenko [4,1] lead to the conclusion that the extra reversible term is irrelevant at late times. We subject the Mazenko closure to systematic numerical tests and show that it is a fairly good approximation at late times. This section is of general interest, since this is a detailed numerical ''test'' of the Mazenko theory for a vector order parameter. In Sec. IV, we investigate the dynamics following a quench to the critical point T_c and show, using a perturbative ϵ expansion, that the reversible term is irrelevant at the Wilson-Fisher fixed point.

II. HEISENBERG MAGNET AND PRECESSIONAL DYNAMICS

The spins ϕ_α $(\alpha=1,2,3)$ in a Heisenberg ferromagnet in three dimensions experience a torque from the joint action of the external field (if present) and the local molecular field. In response the spins precess with a Larmour frequency Ω_L about the total magnetic field. Coupling to various faster degrees of freedom like lattice vibrations or electrons causes a dissipation in the energy and an eventual relaxation towards equilibrium.

This dynamics follows from the generalized Langevin equation (1), and the Poisson algebra Eq. (2),

$$\frac{\partial \phi_\alpha}{\partial t} = -\Gamma(-i\nabla)^\mu \frac{\delta F}{\delta \phi_\alpha} + \Omega_L \epsilon_{\alpha\beta\gamma}\left(\phi_\gamma \frac{\delta F}{\delta \phi_\beta}\right) + \eta_\alpha . \quad (3)$$

The free-energy functional F is taken to be of the Landau form,

$$F[\vec{\phi}] = \int d^3x \left[\frac{\sigma}{2}(\nabla\vec{\phi})^2 - \frac{r}{2}(\vec{\phi}\cdot\vec{\phi}) + \frac{u}{4}(\vec{\phi}\cdot\vec{\phi})^2\right]. \quad (4)$$

The second term in Eq. (3) is clearly the torque $\vec{M}\times\vec{H}$ where $\vec{H}\equiv \delta F/\delta\vec{\phi}$ is the local molecular field.

The free-energy functional is rotationally invariant in spin space and so the Poisson bracket term conserves the total spin. If the dissipation arises from spin-spin interactions, then this will conserve the total spin too and so μ should be taken to be 2. If, however, the dissipation is a consequence of spin-lattice or spin-orbit interactions, then the total spin will not be conserved and so $\mu=0$.

Since the noise correlator is proportional to temperature, we may drop it in our discussion of zero temperature quenches. We then scale space $\mathbf{x}$, time t, and the order parameter $\vec{\phi}$ as

$$\mathbf{x}\to\sqrt{\frac{r}{\sigma}}\mathbf{x},\quad t\to\Gamma r t,\quad \vec{\phi}\to\sqrt{\frac{r}{u}}\vec{\phi}$$

to obtain the equation of motion in dimensionless form,

$$\frac{\partial\vec{\phi}}{\partial t} = \nabla^2\vec{\phi} + \vec{\phi} - (\vec{\phi}\cdot\vec{\phi})\vec{\phi} + g(\vec{\phi}\times\nabla^2\vec{\phi}). \quad (5)$$

The dimensionless parameter $g=(\Omega_L/\Gamma)\sqrt{r/u}$ is the ratio of the precession frequency to the relaxation rate. To get a feel for the values assumed by g, let us set $\Omega_L\sim 10^7$ Hz, $\Gamma\sim 10^6-10^{10}$ Hz, which gives a range of $g\sim 10^{-3}-10$.

III. PHASE ORDERING DYNAMICS: QUENCHES TO $T=0$

Let us now prepare the system initially in the paramagnetic phase and quench to zero temperature. We study the time evolution of the spin configurations as they evolve according to Eq. (5). We calculate the equal time correlator,

$$C(\mathbf{r},t)\equiv\langle\vec{\phi}(\mathbf{r},t)\cdot\vec{\phi}(\mathbf{r}+\mathbf{x},t)\rangle, \quad (6)$$

and the autocorrelator,

$$C(\mathbf{0},t_1=0,t_2)\equiv\langle\vec{\phi}(\mathbf{r},t_1=0)\cdot\vec{\phi}(\mathbf{r},t_2)\rangle, \quad (7)$$

where the angular brackets are averages over the random initial conditions and space. At late times these correlators should attain their scaling form

$$C(\mathbf{r},t)\sim f(r/L(t)), \quad (8)$$

$$C(\mathbf{0},t_1=0,t_2)\sim L(t_2)^{-\lambda}. \quad (9)$$

The length scale $L(t)$ is a measure of the distance between defects and grows with time as $L(t)\sim t^{1/z}$. We compute the scaling function $f(x)$, the growth exponent z, and the autocorrelation exponent λ by (i) simulating the Langevin equation (5) and (ii) Mazenko's closure approximation.

A. Langevin simulation

We discretize Eq. (5) on a simple cubic lattice (with size N ranging from 40^3 to 60^3) adopting a Euler scheme for the derivatives [5]. The space and time intervals have been chosen to be $\Delta x=3$ and $\Delta t=0.01$. With this choice of parameters, we have checked that the resulting coupled map does not lead to any instability. We have also checked that the results remain unchanged on slight variations of Δx and Δt. Unless otherwise specified, all calculated quantities are averaged over 30 uncorrelated initial configurations taken from a uniform distribution with zero mean. Throughout our simulation we have used periodic boundary conditions.

The scaling of the energy density,

$$\varepsilon = \frac{1}{V}\int d\mathbf{r}\langle[\nabla\phi(\mathbf{r},t)]^2\rangle \quad (10)$$

can be used to determine the dynamic exponent z. For vector order parameters, $\varepsilon\sim L(t)^{-2}$ at late times, where $L(t)$ is the length scale beyond which the field of the defect is screened by other defects. Figure 1 shows a log-log plot of the energy density as a function of t for $g=0$, 0.5, 1, 2 on a 60^3 lattice. The error bars are smaller than the size of the symbols. Up to these times ($t=16\,000$), there is no evidence of finite size effects. The slight curvature seen in the data (especially for larger g) is due to finite time corrections. The bold line corresponds to $A/(t+t_0)$ where A and t_0 are varied to give the best fit to the data. This shows that the data gathered over 1.5 decades gives a $z=2$, *independent of* g.

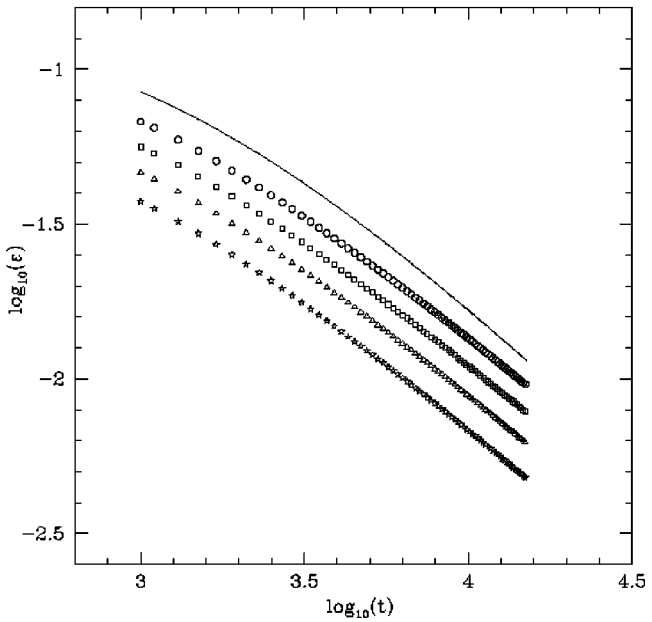

FIG. 1. Log-log plot of the energy density ε vs t for various values of g, $g=0$ ($\bigcirc$), $g=0.5$ ($\square$), $g=1$ ($\triangle$), $g=2$ ($\star$). The straight line is a fit (see text).

We next calculate $C(r,t)$ at these late times for different values of g. Figures 2(a)–2(b) are scaling plots of $C(r,t)$ versus $r/t^{1/2}$ [see Eq. (8)] for $g=0$ and $g=1$ on a 40^3 lattice (finite size effects manifest at $t>12\,000$). The domain size $L(t)$ extracted from $C(r=L(t),t)=C(0,t)/2$, scales as $t^{1/z}$, where the exponent is again $z=2$ (within statistical errors) and independent of g. Figure 3 shows that the scaling function $f(x)$ is also *independent of* g, for $g=0$, 0.5, 1, 2. This scaling function is compared (bold line in Fig. 3) with the approximate BPT scaling function for $g=0$ [6], $f(x)=(3\gamma/2\pi)[B(2,1/2)]^2F(1/2,1/2,5/2;\gamma^2)$ where $\gamma=\exp(-x^2/8)$ and B and F are the beta and the hypergeometric functions, respectively.

At larger values of g, finite size effects become very prominent. This can be seen from the form of the late-time $C(r,t)$ for $g=5$ (Fig. 4), simulated on a 50^3 lattice averaged over 7 initial configurations. The correlation function crosses zero at large r, dips through a minimum, and then asymptotically goes to zero [of course $\int C(r,t)>0$]. It is clear from the figure that at these times, $C[r/L(t)]$ for $g=5$ would be qualitatively different from the scaling function of Fig. 3. However, notice that the dip decreases with increasing time. This would suggest that the dip might disappear at late times [7], and that the resulting scaling function would be identical to Fig. 3. In the next paragraph we will argue that this dip is a preasymptotic feature and disappears in the scaling limit. This will allow us to conclude that the scaling function $f(x)$ is indeed independent of g.

At very late times, the order parameter field has totally relaxed with respect to defect cores. Preasymptotic configurations typically consist of spin wave excitations interspersed between slowly moving defects separated by a distance $L(t)\gg\xi$, the size of the defect core. Decomposing $\vec{\phi}$ into a singular (defect) part $\vec{\phi}_{\rm sing}$ and a smooth (spin wave) part $\vec{\phi}_{\rm sm}$, we calculate the preasymptotic correlation function

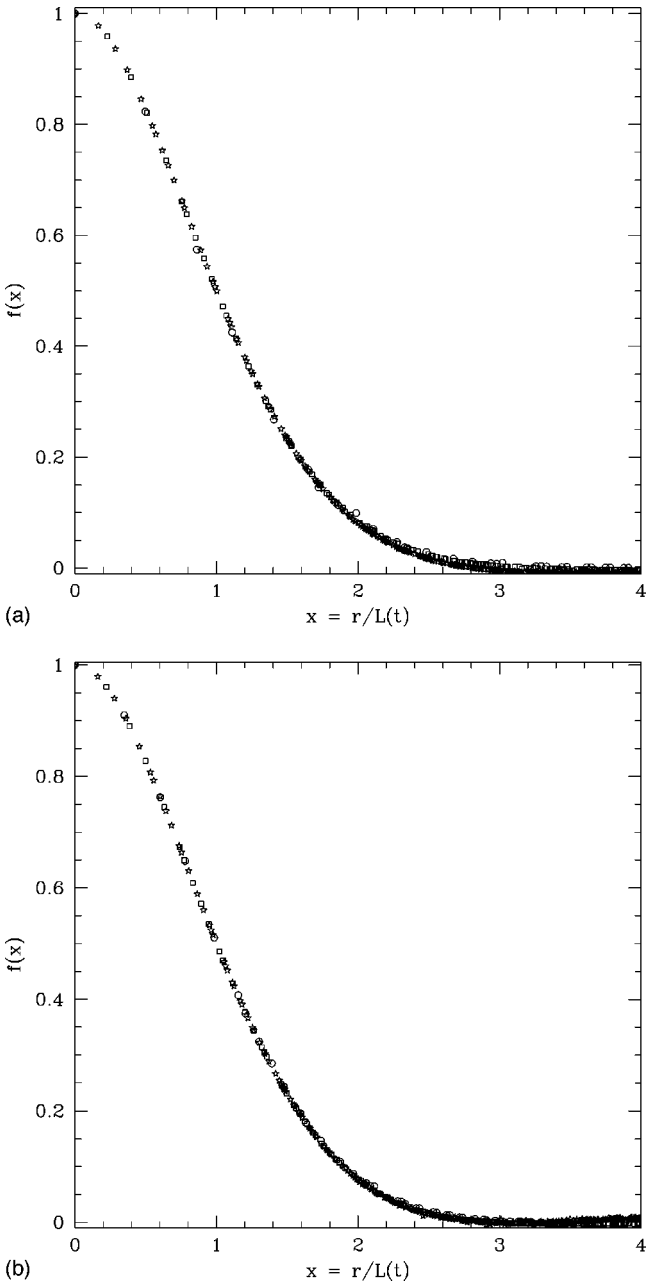

FIG. 2. (a) The scaling function $f(x)$ vs $x\equiv r/t^{1/2}$ for $g=0$. Data are taken at $t=1000$ ($\bigcirc$), $t=5000$ ($\triangle$), and $t=10\,000$ ($\star$). Error bars are smaller than the size of symbols. (b) $f(x)$ vs $x\equiv r/t^{1/2}$ for $g=1$. Data are taken at $t=2000$ ($\bigcirc$), $t=5000$ ($\triangle$), and $t=10\,000$ ($\star$). Error bars as in (a).

within a perturbative analysis (see Appendix for details). The computed correlation function exhibits a dip at $r^2/t\sim(1+g^2)/g$, which disappears algebraically in time (see Appendix). The amplitude of this dip increases with increasing g. The dip eventually goes away with a relaxation time that scales as (t_* is the time at which the $g=0$ correlation function first exhibits scaling)

$$\tau(g)=t_*(1+g^2). \tag{11}$$

The crossover time $\tau(g)$ is estimated to be (taking $t_*=1000$ for the 40^3 system) $\tau(g=1)=2000$, $\tau(g=2)=5000$, and $\tau(g=5)=26\,000$. The crossover times for g

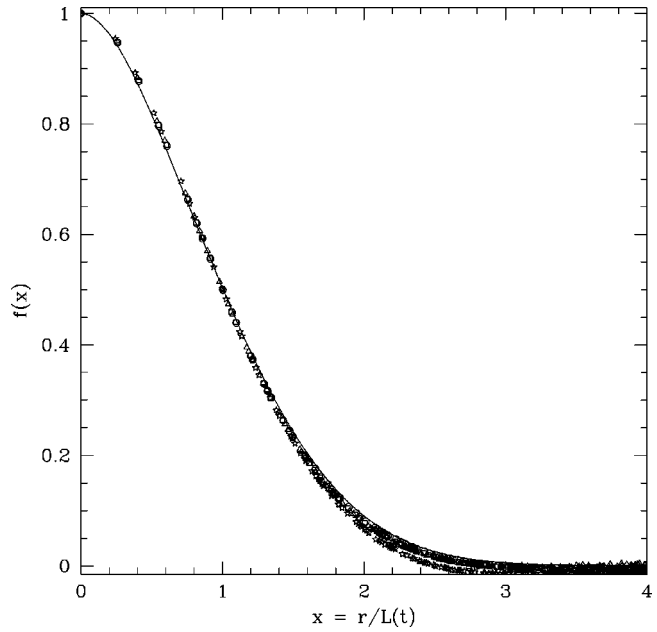

FIG. 3. $f(x)$ vs $x \equiv r/t^{1/2}$ for different values of g [$g=0$ (○), 0.5 (□), 1 (△), 2 (⋆)]. The data for $g=2$ were obtained from a simulation on a 50^3 lattice averaged over 7 configurations. The continuous curve is the approximate analytical form defined in the text [6].

$\geqslant 5$ are much larger than the largest time reached in our simulation. Figure 5 is a plot of preasymptotic $C(r,t) = C_{\rm sing} + C_{\rm sm}$ at a fixed time where $C_{\rm sing}$ is given by the BPT form [6] and $C_{\rm sing}$ takes the form derived in the appendix. Two adjustable parameters related to the length scale and the amplitude of the spin wave have been tuned to obtain excellent fits to the numerical data. Based on these arguments we conclude that the scaling function $f(x)$ is independent of g.

We now compute the autocorrelation function $C(0,0,t)$ and extract the exponent λ [see Eq. (9)]. The time t ranges

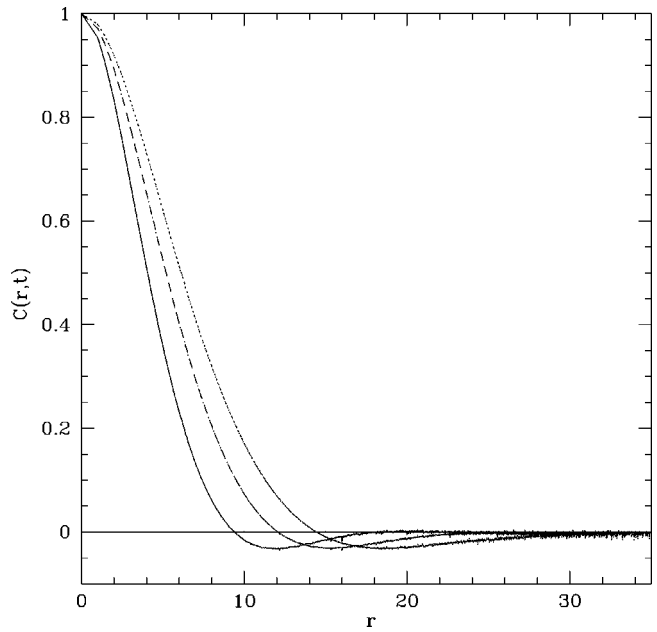

FIG. 4. The correlation function $C(r,t)$ vs r for $g=5$ at various times $t=3000$ (−), $t=5000$ (− · − ·), $t=7000$ (· · ·). Note that the dip gets smaller as time progresses. Error bars as in Fig. 2(a).

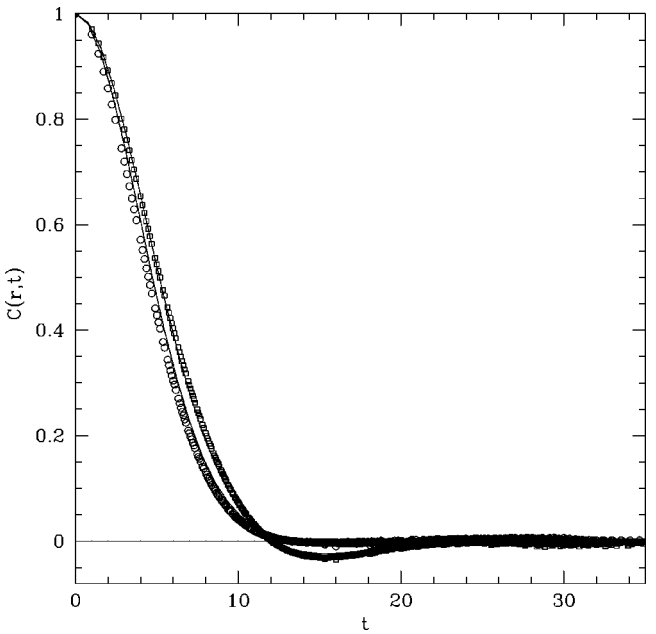

FIG. 5. Preasymptotic $C(r,t)$ for $g=1$ and 5 (bold lines) calculated in Appendix A. Note the excellent fit to data for $g=1$ (○), $g=5$ (□).

from 4000 to 16 000 for the 60^3 lattice (averaged over 50 initial configurations), well into the scaling regime for the one-time correlator. Figure 6 is log-log plots of $C(0,0,t)$ versus t for $g=0$, 0.5, 1, and 2. It is difficult to give a precise value of the decay exponent λ, since as can be seen from Fig. 7, the ''effective'' λ varies by about 3% over half a decade. However, it is evident from the bold line in Fig. 6, which corresponds to $A(t+t_0)^{-\lambda/2}$ (A and t_0 are varied to give the best fit to the overall data), that the value of λ is independent of g. A fit to each data set for a given g, obtains

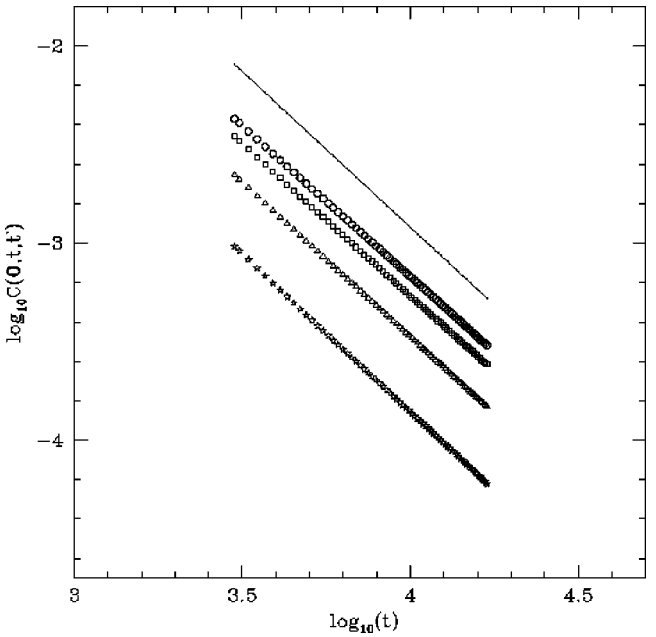

FIG. 6. Log-log plot of the autocorrelation function $C(0,0,t)$ vs t for $g=0$ (○), 0.5 (□), 1 (△), 2 (⋆). The straight line is a fit $A(t+t_0)^{-\lambda/2}$, where λ has been chosen to be the Mazenko value -1.587.

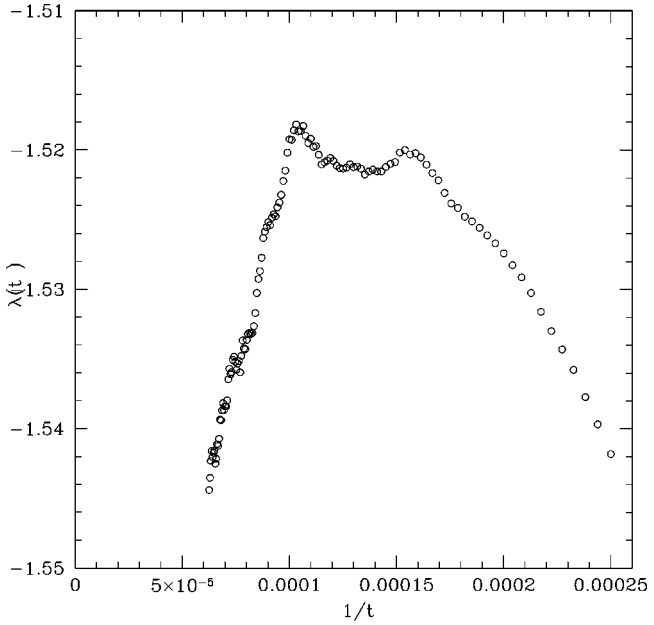

FIG. 7. Effective λ as a function of $1/t$ for $g=0$.

the following values for the exponent λ—$\lambda(g=0)=1.526\pm0.007$, $\lambda(g=0.5)=1.521\pm0.008$, $\lambda(g=1)=1.55\pm0.01$, and $\lambda(g=2)=1.55\pm0.02$. The numerical values listed above can be compared to the Mazenko closure estimate of 1.587 for $g=0$ [1]. These values obey the Huse-Fisher bound $\lambda>d/2$.

It is clear that finite size effects set in at later times. As discussed in [8], finite size effects will be relevant when the spread in $C(0,0,t)$ [given by $\Delta C(0,0,t)\sim N^{-3/2}$] is of order $C(0,0,t)$ itself. This will happen when $L^{-\lambda}\sim N^{-3/2}$. The fact that the numerically computed λ increases marginally with g indicates that finite size effects are more apparent for larger g. This is consistent with our discussion on the effects of finite size on single-time correlators.

We end this section with the following assertion based on our careful numerics. The exponents z and λ and the scaling function $f(x)$ are seen to be independent of the torque g. This implies that the torque is irrelevant to the late-time dynamics at $T=0$. In the next section, we will apply the approximate method of Mazenko to this problem and arrive at the same conclusion.

B. Application of the Mazenko closure scheme

Of the variety of approximate schemes devised to evaluate the form of the scaling function, the closure scheme introduced by Mazenko [4] is amenable to systematic improvement [1,9]. We shall use this closure scheme to determine the scaling form $f(x)$ and show that it is independent of g. The method consists of trading the order parameter $\vec{\phi}(\mathbf{r},t)$ which is singular at defect sites, for an everywhere smooth field $\vec{m}(\mathbf{r},t)$, defined by a nonlinear transformation

$$\vec{\phi}(\mathbf{r},t)=\vec{\sigma}(\vec{m}(\mathbf{r},t)). \tag{12}$$

At late times, the magnitude of $\vec{\phi}$ saturates to its equilibrium value almost everywhere except near the defect cores. This suggests that the appropriate choice for the nonlinear function $\vec{\sigma}$ is an equilibrium defect profile,

$$\frac{1}{2}\nabla_m^2\vec{\sigma}(\vec{m}(\mathbf{r},t))=V'(\vec{\sigma}(\vec{m}(\mathbf{r},t))), \tag{13}$$

where $V'(x)\equiv-\vec{x}+(\vec{x}\cdot\vec{x})\vec{x}$. This choice allows for a natural interpretation of $\vec{m}$ (in the vicinity of a defect) as the position vector from a defect core. The simplest nontrivial solution of Eq. (13) is the hedgehog configuration,

$$\vec{\sigma}(\vec{m}(\mathbf{r},t))=\frac{\vec{m}(\mathbf{r},t)}{|\vec{m}(\mathbf{r},t)|}g(|\vec{m}|), \tag{14}$$

where $g(0)=0$ and $g(\infty)=1$. Equation (5) can be used to derive an equation for the correlation function $C(12)\equiv\langle\phi(\mathbf{r}_1,t_1)\cdot\phi(\mathbf{r}_2,t_2)\rangle$. Substituting for ϕ [Eqs. (12) and (14)] in the right hand side of the resulting equation, we get

$$\partial_t C(12)=\nabla_1^2C(12)+\langle\vec{\sigma}(\vec{m}(2))\cdot V'(\vec{\sigma}(\vec{m}(1)))\rangle + g\langle\vec{\sigma}(\vec{m}(2))\cdot\vec{\sigma}(\vec{m}(1))\times\nabla^2\vec{\sigma}(\vec{m}(2))\rangle. \tag{15}$$

So far no approximation has been made, but further progress seems impossible without one. Now along with Mazenko, we make the assumption that each component of $\vec{m}(\mathbf{r},t)$ is an independent Gaussian field with zero mean at all times. This implies that the joint probability distribution $P(12)\equiv P(\vec{m}(1),\vec{m}(2))$ is a product of separate distributions for each component and is given by [1]

$$\prod_\alpha \mathcal{N}\exp\left\{-\frac{1}{2(1-\gamma^2)}\left(\frac{m_\alpha^2(1)}{S_0(1)}+\frac{m_\alpha^2(2)}{S_0(2)}-\frac{2\gamma m_\alpha(1)m_\alpha(2)}{\sqrt{S_0(1)S_0(2)}}\right)\right\}, \tag{16}$$

where

$$\mathcal{N}=\frac{1}{2\pi\sqrt{(1-\gamma^2)S_0(1)S_0(2)}}$$

and

$$\gamma\equiv\gamma(12)=\frac{C_0(12)}{\sqrt{S_0(1)S_0(2)}}.$$

The joint distribution has been written in terms of the second moments $S_0(1)=\langle m_\alpha(1)^2\rangle$, $S_0(1)=\langle m_\alpha(1)^2\rangle$, and $C_0(12)=\langle m_\alpha(1)m_\alpha(2)\rangle$.

With this assumption, the right hand side of Eq. (15) simplifies to

$$\frac{\partial C(12)}{\partial t_1}=\nabla^2C(12)+\frac{\gamma}{2S_0(1)}\frac{\partial C(12)}{\partial\gamma} + g\langle\vec{\sigma}(\vec{m}(2))\cdot\vec{\sigma}(\vec{m}(1))\times\nabla^2\vec{\sigma}(\vec{m}(2))\rangle. \tag{17}$$

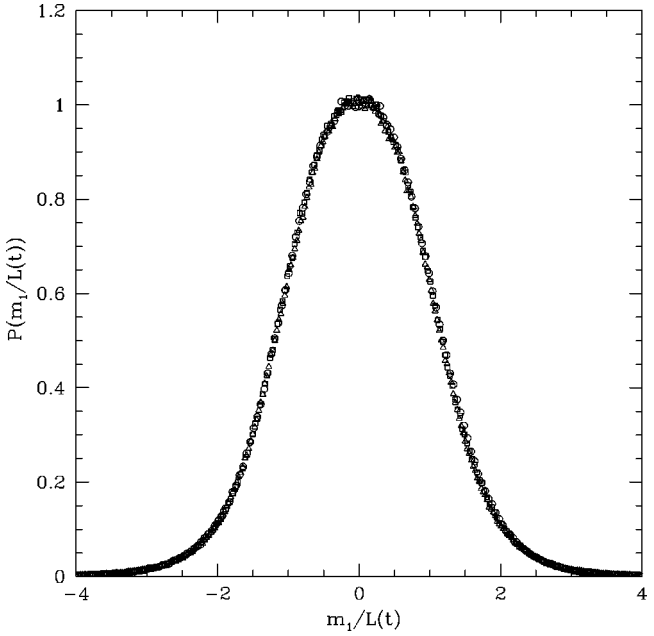

FIG. 8. Single point distribution of $P(m_1)$ for $g=0$ at different times: $t=5000$ (○), $t=10\,000$ (□), $t=15\,000$ (△). The distribution scales in the variable m_1/L, where $L(t)=\sqrt{S_0(t)}$.

It is clear that since $P(\vec{m}(1),\vec{m}(2))=P(-\vec{m}(1),-\vec{m}(2))$, the last term, which is odd in $\vec{m}$, drops out. The resulting equation is identical to the purely dissipative one, showing that the torque is irrelevant at late times. This conclusion, consistent with our earlier numerics, is a direct consequence of the Mazenko closure approximation.

C. Justification of the Mazenko approximation for vector order parameters

In this section we will subject the above stated assumptions of the Mazenko closure scheme to systematic numerical tests. We will do this by numerically solving the Langevin equation (5) by the method outlined in Sec. III A. Knowing $\vec{\phi}(\mathbf{r},t)$, one can compute $\vec{m}(\mathbf{r},t)$ by inverting Eq. (14). This is facilitated by choosing

$$g(|\vec{m}|)=\frac{|\vec{m}|}{\sqrt{1+\vec{m}\cdot\vec{m}}}, \tag{18}$$

which is consistent with the boundary conditions for $g(x)$ mentioned in the previous section. The resulting ansatz for $\vec{\sigma}$,

$$\vec{\sigma}(\vec{m}(\mathbf{r},t))=\frac{\vec{m}}{\sqrt{1+\vec{m}\cdot\vec{m}}}, \tag{19}$$

can be easily inverted. We calculate both the single point probability distribution $P(\vec{m}(\mathbf{r},t))$ and the joint probability distribution $P(12)$ in the scaling regime and compare with the Mazenko assumption. In what follows all probability distributions have been computed on a 45^3 lattice and averaged over 100 initial configurations. We shall display the distributions for $g=0$ and $g=1$. We have collected data in the scaling regime from $t=2000$ to $t=15\,000$, after which finite size effects set in.

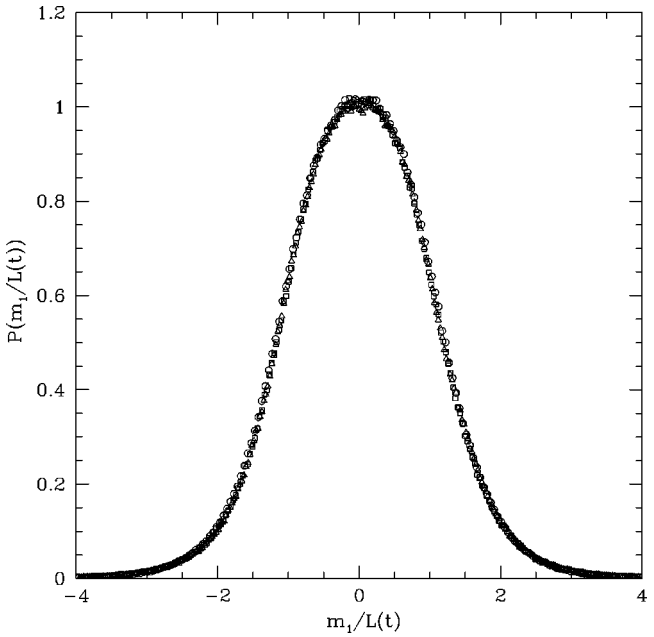

FIG. 9. Same as Fig. 8, but for $g=1$ for times $t=5000$ (○), $t=10\,000$ (□), $t=15\,000$ (△).

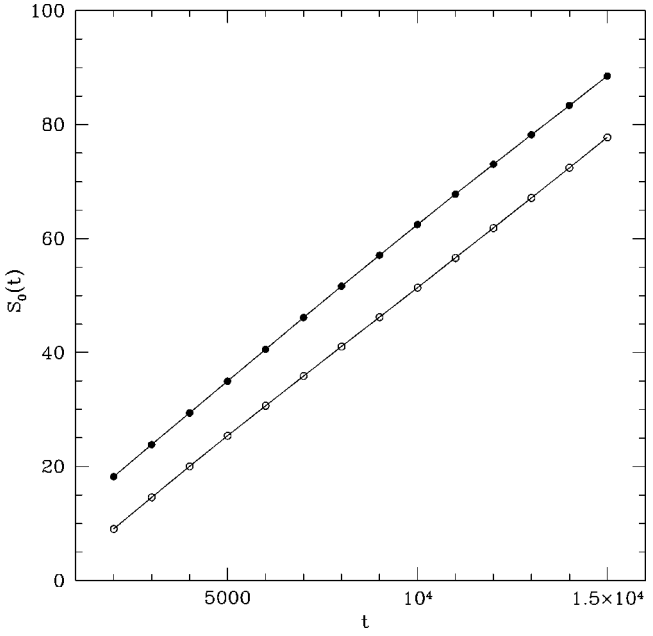

FIG. 10. Linear growth of $S_0(t)$ with t for $g=0$(○) and $g=1$(●).

Figure 8 and 9 are scaling plots of $P(m_1(\mathbf{r},t))$ at $g=0$ and $g=1$, respectively. In accordance with the Mazenko assumption, the scaling variable has been taken to be $m_1/\sqrt{S_0(t)}$, where $S_0(t)=\langle m_1(r,t)^2\rangle$. A plot of $S_0(t)$ (for both $g=0$ and 1) versus t (Fig. 10) shows a linear growth over a decade, consistent with $z=2$. The scaled distribution $P(m_1)$ is also seen to be the same for $g=0$ and $g=1$ (Fig. 11), suggesting that it is independent of g.

Though the distribution grossly resembles a Gaussian at late times, a closer inspection shows systematic deviations at

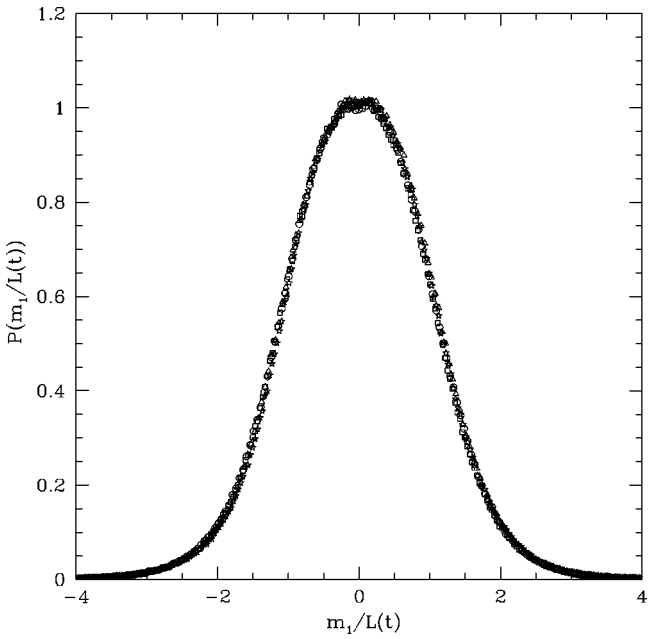

FIG. 11. Scaling plot of $P(m_1)$ is independent of g. Data taken for $g=0$ [$t=5000$ (○), $t=10\,000$ (□)] and $g=1$ [$t=5000$ (△), $t=10\,000$ (⋆)].

small values of m_1 (Fig. 11). The distribution seems to be flatter than a Gaussian when $m_1 \approx 0$. This is clearly visible in a plot of $-\ln\{-\ln[P(m_1^2/S_0)]\}$ versus $\ln(m_1^2/S_0)$, which shows that the distribution deviates from a Gaussian for small m_1 (Fig. 12). These findings are consistent with a similar analysis done on a scalar order parameter [10].

We now study the two point distribution $P(\vec{m}(1),\vec{m}(2))$. Equation (16) implies that in the variables

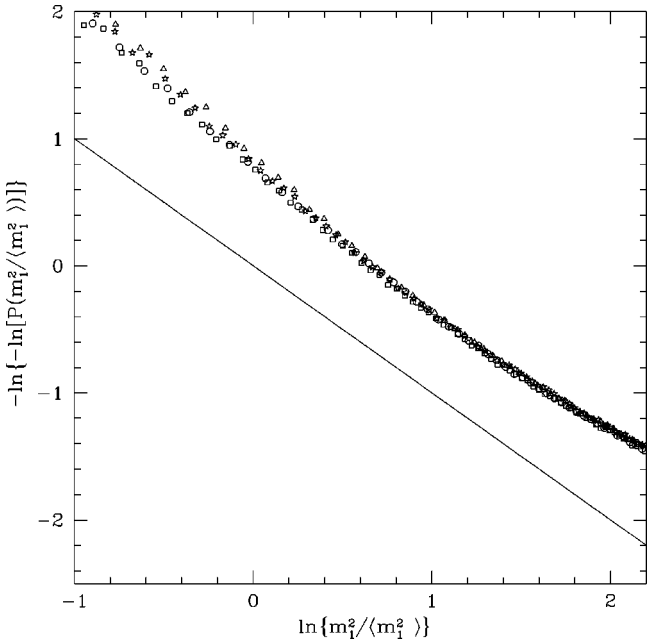

FIG. 12. Plot of $-\ln\{-\ln[P(m_1^2/S_0)]\}$ vs $\ln(m_1^2/S_0)$ for $g=0$ [$t=5000$ (○), $t=10\,000$ (□)] and $g=1$ [$t=5000$ (△), $t=10\,000$ (⋆)]. The line with slope -1 drawn for comparison, highlights the deviation of the data from a Gaussian at smaller m_1.

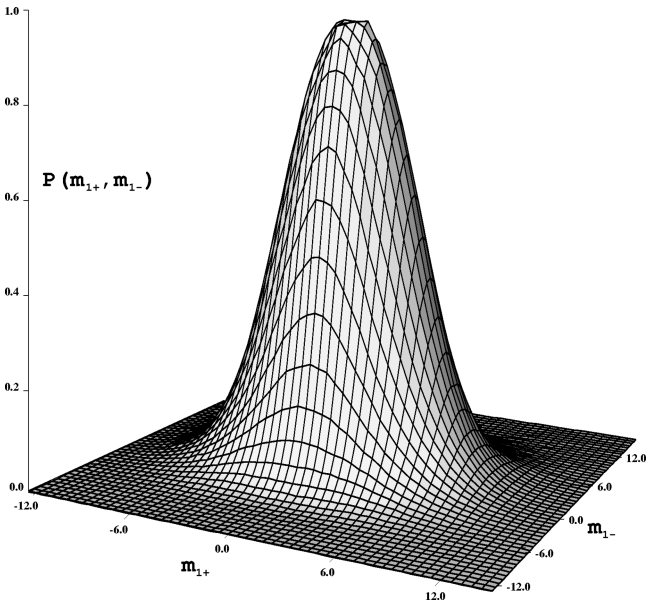

FIG. 13. Joint probability distribution $P[\vec{m}_+(12),\vec{m}_+(12)]$ for $g=0$ at $t=5000$ and $|\mathbf{r}_1-\mathbf{r}_2|=4\sqrt{3}$.

$$\vec{m}_\pm(12)=\frac{1}{2}\left(\frac{\vec{m}(1)}{\sqrt{S_0(1)}}\pm\frac{\vec{m}(2)}{\sqrt{S_0(2)}}\right)[S_0(1)S_0(2)]^{1/4},$$

the distribution $P(12)=P(\vec{m}_+(12))P(\vec{m}_-(12))$, where

$$P(\vec{m}_\pm(12))=\prod_\alpha \sqrt{\mathcal{N}}\exp\left\{-\frac{m_{\alpha\pm}^2}{(1\pm\gamma)\sqrt{S_0(1)S_0(2)}}\right\}. \tag{20}$$

We compute $P(m_{\alpha+}(12),m_{\alpha-}(12))$ at $t_1=t_2=t$ in the scaling regime. A plot of $P(m_{1+},m_{1-})$ (Fig. 13) for $|\mathbf{r}_1-\mathbf{r}_2|=4\sqrt{3}$ looks like a product of two Gaussian distributions. To check this we compute the difference

$$\Delta(m_{\alpha+}(12),m_{\alpha-}(12))=P(m_{\alpha+}(12),m_{\alpha-}(12))-P(m_{\alpha+}(12))P(m_{\alpha-}(12)),$$

which should be zero everywhere if the Mazenko approximation were to hold.

Figure 14 shows a surface plot of the difference $\Delta(m_{1+}(12),m_{1-}(12))$, magnified 10^5 times. It is clear that $\Delta(m_{1+}(12),m_{1-}(12))$ is zero everywhere except in the region close to the origin, where the maximum deviation from 0 is around 10^{-5}. The situation is similar for $g=1$. We now compute $P(m_{1+}(12))$ and $P(m_{1-}(12))$, and find that the scaled distributions are the same for $g=0$ and $g=1$. Figures 15 and 17 are scaling plots of $P(m_{1+})$ and $P(m_{1-})$, respectively , and indicate that the scaling function is independent of g. Moreover the distribution looks like a Gaussian, in accordance with the Mazenko theory. Figures 16 and 18 are plots of $-\ln\{-\ln[P(m_{1\pm}^2(12)/\langle m_{1\pm}^2(12)\rangle)]\}$ versus $\ln[m_{1\pm}^2(12)/\langle m_{1\pm}^2(12)\rangle]$. The deviation from a straight line when $m_{1\pm}\approx 0$ indicates that the distributions differ slightly from a Gaussian. Note that the data for small $m_{1\pm}$ in Figs. 16

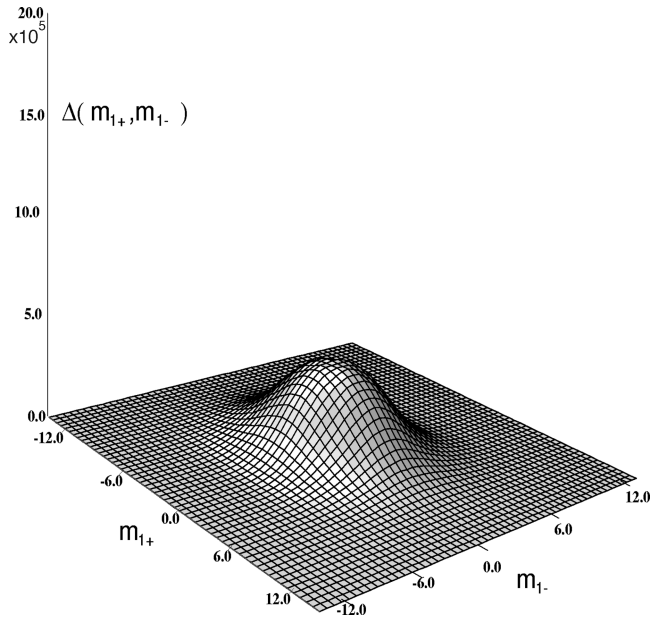

FIG. 14. Surface plot of $\Delta[m_{1+}(12),m_{1-}(12)]$ (magnified 10^5 times) for $g=0$ at $t=5000$ and $|\mathbf{r}_1-\mathbf{r}_2|=4\sqrt{3}$.

and 18 do not quite scale and so it is likely that in the computation of the joint-probability distribution, we have not yet reached the scaling regime.

In conclusion, we have shown, by computing the single and the two-point probability distributions, that the Mazenko closure scheme is a fairly good approximation at late times with possible deviations when $m_\alpha \approx 0$. This study justifies the use of the Mazenko approximation in the evaluation of the correlation functions and hence the results of the previous section. This constitutes the first serious numerical check on the assumptions of the Mazenko scheme for vector order parameters.

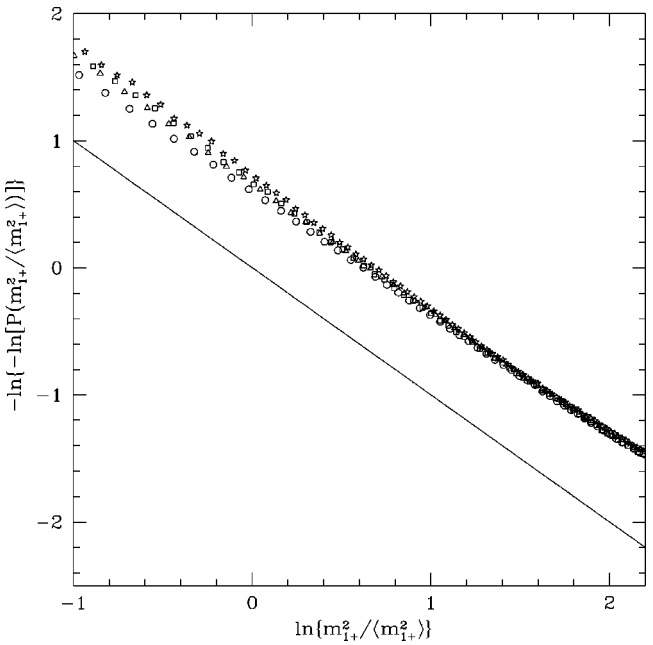

FIG. 16. $P(m_{+1}/L_+)$ shows deviation from Gaussian for small m_+. Data are shown for $g=0$ [$t=5000$ (○), $t=10\,000$ (□)] and $g=1$ [$t=5000$ (△), $t=10\,000$ (⋆)].

IV. PHASE ORDERING DYNAMICS: QUENCHES TO $T=T_c$

We now quench from the high-temperature paramagnetic phase to the critical point T_c, and ask whether the spin precession changes the late time dynamical behavior. More precisely, we would like to know whether the torque term g is relevant at the Wilson-Fisher fixed point corresponding to the pure $g=0$ Heisenberg model with nonconserved dynamics.

This can be done by power counting [11] to $O(\epsilon^2)$ at the

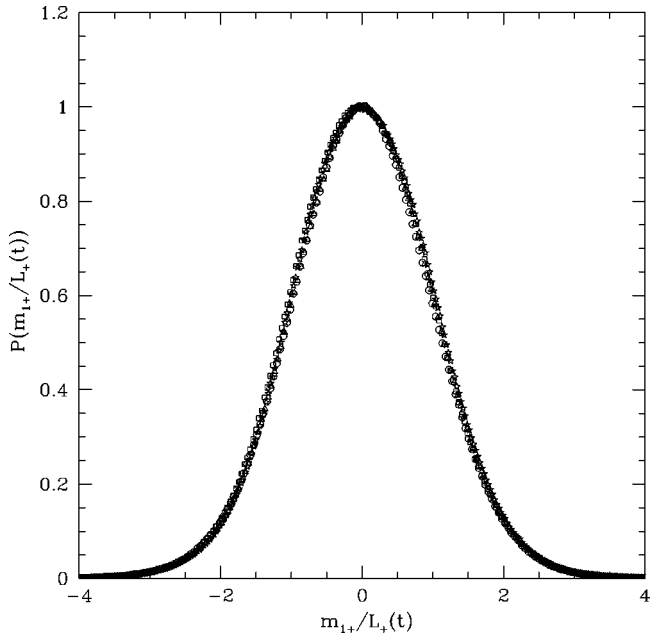

FIG. 15. Scaling plot of $P(m_{+1}/L_+)$, where $L_+=\sqrt{\langle m^2_{+1}(\mathbf{r},t)\rangle}$, for $g=0$ [$t=5000$ (○), $t=10\,000$ (□)] and $g=1$ [$t=5000$ (△), $t=10\,000$ (⋆)].

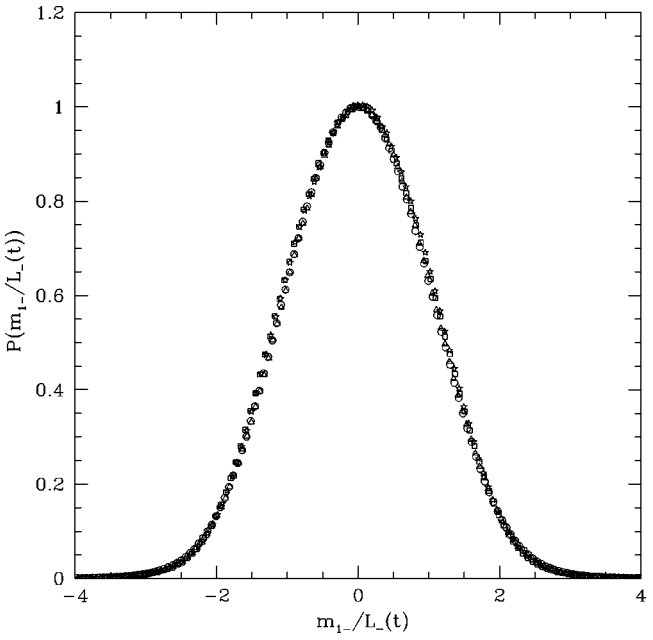

FIG. 17. Scaling plot of $P(m_{-1}/L_-)$, where $L_-=\sqrt{\langle m^2_{-1}(\mathbf{r},t)\rangle}$, for $g=0$ [$t=5000$ (○), $t=10\,000$ (□)] and $g=1$ [$t=5000$ (△), $t=10\,000$ (⋆)].

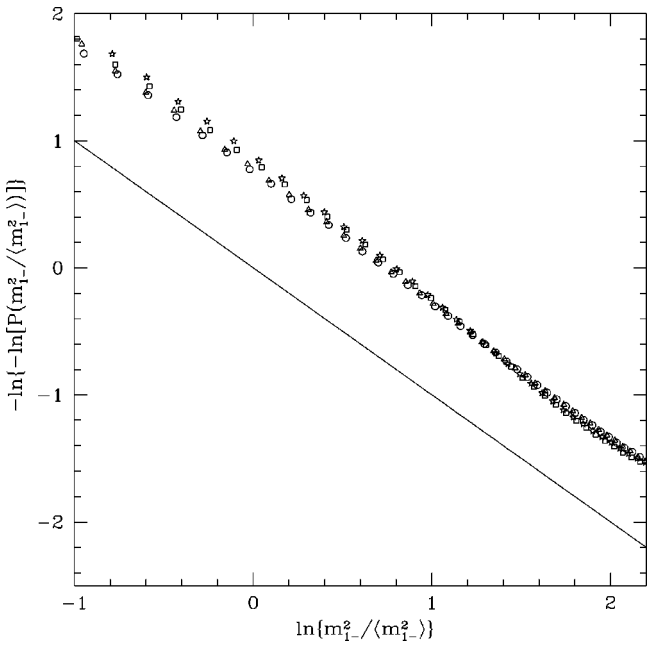

FIG. 18. $P(m_{-1}/L_{-})$ shows deviation from Gaussian for small m_{-1}. Data are shown for $g=0$ [$t=5000$ (○), $t=10\,000$ (□)] and $g=1$ [$t=5000$ (△), $t=10\,000$ (⋆)].

Wilson-Fisher fixed point $r^*=-(5/22)\Lambda^2\epsilon$, $u^*=8\pi^2\epsilon/11$ (Λ is the ultraviolet cutoff). Dimensional analysis provides the scaling dimension $[g]=d/2+1-z+\eta/2$. At the Wilson-Fisher fixed point $z=2+c\,\eta$, where $c=6\ \ln(4/3)-1$, and $\eta=(5/242)\epsilon^2$. This implies that above $d=2$, the torque term is irrelevant. In $d=1$, the torque is relevant, as can be seen by an explicit solution of the Langevin equation (5) in one spatial dimension.

V. CONCLUSIONS

We have investigated the effect of reversible Possion bracket terms in a generalized Langevin equation on the phase ordering dynamics at late times. The dynamics of such systems can be classified by the structure of the Poisson brackets. Here we have made a detailed study of the nonconserved dynamics of an order parameter whose components obey a Lie algebra. A common example is the nonconserved dynamics of a Heisenberg magnet. The dynamics consists of two parts — an irreversible dissipation into a heat bath and a reversible precession induced by a torque due to the local molecular field. For quenches to zero temperature, we have shown, both numerically (Langevin simulation) and analytically (approximate closure scheme due to Mazenko), that the torque is irrelevant at late times. The Mazenko closure was subject to critical numerical tests and was shown to perform well at late times (apart from small deviations). For quenches to T_c, we show to $O(\epsilon^2)$ that the torque is irrelevant at the Wilson-Fisher fixed point.

In a future paper we plan to investigate the effect of the reversible torque on the conserved dynamics of the Heisenberg magnet in three dimensions. We will show that the torque is relevant both for quenches to $T=0$ and $T=T_c$.

APPENDIX

In this Appendix we study the effect of spin wave excitations on the time dependent preasymptotic equal-time correlation function. We would like to show that inclusion of such excitations in the correlation function $C(r,t)$ leads to a dip at preasymptotic times when $g\neq 0$, which eventually relaxes. As suggested in Sec. III A, at very late times, the order parameter field has totally relaxed with respect to defect cores. Preasymptotic configurations typically consist of spin wave excitations interspersed between slowly moving defect cores. These defect cores are separated by a typical distance $L(t)\gg\xi$, the size of the defect core. In general one can decompose $\vec{\phi}(\mathbf{r},t)=\vec{\phi}_{\rm sing}(\mathbf{r},t)+\vec{\phi}_{\rm sm}(\mathbf{r},t)$, where the singular part $\vec{\phi}_{\rm sing}$ parametrizes defect configurations while the smooth part $\vec{\phi}_{\rm sm}$ is a linear combination of spin waves of wavevector $\mathbf{k}$, $\vec{\phi}_{\rm sm}(\mathbf{r},t)=V^{-1/2}\Sigma\,\vec{\phi}_{\mathbf{k}}^{\rm sm}(t)e^{i\mathbf{k}\cdot\mathbf{r}}$. The preasymptotic correlation function will thus have three contributions — $C_{\rm sing}\equiv\langle\vec{\phi}_{\rm sing}(0,t)\cdot\vec{\phi}_{\rm sing}(\mathbf{r},t)\rangle$, $C_{\rm sm}\equiv\langle\vec{\phi}_{\rm sm}(0,t)\cdot\vec{\phi}_{\rm sm}(\mathbf{r},t)\rangle$ and the scattering of spin waves from slowly moving defects $C_{\rm scat}\equiv\langle\vec{\phi}_{\rm sm}(0,t)\cdot\vec{\phi}_{\rm sing}(\mathbf{r},t)\rangle$. At late times of course $\vec{\phi}_{\mathbf{k}}^{\rm sm}(t)\rightarrow 0$, and $\vec{\phi}_{\rm sing}$ can be traded off for the auxilliary field $\vec{m}$ within the Mazenko approach. Thus the $C_{\rm sing}(r,t)$ part of the correlation function is given by the solution of Eq. (17) or the BPT form [6].

The smooth part of the correlation function $C_{\rm sm}(r,t)$ can be estimated from a perturbative calculation, wherein the defects separated by a distance $L\gg\xi$ are taken to be static (justified *post priori*). We shall see that the dip is a result of this smooth part. Confining our attention to a single domain of size L, we can split the smooth $\vec{\phi}_{\rm sm}$ into transverse and longitudinal components about the well-defined broken symmetry axis taken to be along $\alpha=3$. Thus $\phi_\alpha^{\rm sm}(\mathbf{r},t)=\phi_{\rm eq}\delta_{\alpha 3}+u_\alpha(\mathbf{r},t)$, where the equilibrium magnetization $\phi_{\rm eq}=1$.

Consider an initial smooth localized pulse in the interior of this domain of the form $u_1(\mathbf{r},0)=u_2(\mathbf{r},0)=[u(0)/(2\sigma)^3\pi^{3/2}]e^{-r^2}/4\sigma 2$ and $u_3(\mathbf{r},0)=[u_3(0)/(2\omega)^3\pi^{3/2}]e^{-r^2}/4\omega^2$, where the widths σ, $\omega\ll L$ and $u(0)$, $u_3(0)\ll 1$. The equation for u_α can be read out from Eq. (5),

$$\frac{\partial u_\alpha}{\partial t}=\nabla^2 u_\alpha-g\epsilon_{\alpha\beta 3}\nabla^2 u_\beta-2u_3\delta_{\alpha 3}-(u_\beta u_\beta)\delta_{\alpha 3}-2(u_\alpha u_\beta)\delta_{\beta 3}+g\epsilon_{\alpha\beta\gamma}u_\beta\nabla^2 u_\gamma-u_\beta u_\beta u_\alpha. \quad \text{(A1)}$$

To solve this equation perturbatively, we multiply the nonlinear terms in Eq. (A1) by an arbitrary real parameter $\epsilon(\leqslant 1)$ and express $u_\alpha(\mathbf{r},t)$ as $\Sigma_{n=0}^{n=\infty}\epsilon^n u_\alpha^{(n)}(\mathbf{r},t)$. The initial conditions for $u_\alpha^{(n)}(\mathbf{r},0)$ follow from $u_\alpha(r,0)$. We are interested in solutions that decay as $t\rightarrow\infty$. Convergence of the perturbation series at $\epsilon=1$ is guaranteed by the smallness of the initial deviation and because higher-order terms in the expansion decay faster. To $O(\epsilon^0)$, the spin waves do not interact and

$$\frac{\partial u_\alpha^{(0)}}{\partial t}=\nabla^2 u_\alpha^{(0)}-g\epsilon_{\alpha\beta 3}\nabla^2 u_\beta^{(0)}-2u_3^{(0)}\delta_{\alpha 3}. \quad \text{(A2)}$$

The equations for $u_1^{(0)}$ and $u_2^{(0)}$ decouple in the variables $u_\pm^{(0)}=(u_1^{(0)}\pm iu_2^{(0)})/2$, giving rise to two precessing goldstone modes in the transverse direction and an exponentially decaying mode in the longitudinal direction. Thus,

$$u_{\pm}^{(0)}(\mathbf{r},t)=\frac{(1\pm i)u(0)}{16[\pi t(1\pm ig)]^{3/2}}\exp\left(-\frac{r^2}{4(1\pm ig)t}\right)$$

and

$$u_3^{(0)}(\mathbf{r},t)=\frac{u_3(0)}{8(\pi t)^{3/2}}\exp\left(-\frac{r^2}{4t}-2t\right) \tag{A3}$$

are the asymptotic solutions to $O(\epsilon^0)$.

To $O(\epsilon)$, the dynamical equations in the transverse variables are given by

$$\frac{\partial u_{\pm}^{(1)}}{\partial t}=(1\pm ig)\nabla^2 u_{\pm}^{(1)}-2u_3^{(0)}u_{\pm}^{(0)}\pm ig(u_3^{(0)}\nabla^2 u_{\pm}^{(0)} - u_{\pm}^{(0)}\nabla^2 u_3^{(0)})-[4u_+^{(0)}u_-^{(0)}+(u_3^{(0)})^2]u_{\pm}^{(0)}. \tag{A4}$$

The last two terms are subdominant in $1/t$ and $u(0),u_3(0)$ respectively, and so the transverse correlator to $O(\epsilon)$ is given by

$$C_{\rm sm}^{\perp}(\mathbf{r},t)=\frac{1}{2}\langle u_+(\mathbf{x},t)u_-(\mathbf{x}+\mathbf{r},t)+u_+(\mathbf{x}+\mathbf{r},t)u_-(\mathbf{x},t)\rangle \sim \frac{A_1}{t^{3/2}}\exp\left(-\frac{r^2}{8t}\right)+\frac{A_2e^{-2t}}{t^3}\exp\left(-\frac{r^2}{2t(3+g^2)}\right)\times\left\{\cos\left(\frac{gr^2}{4t(3+g^2)}+\pi/4\right)\right\}, \tag{A5}$$

where $A_1\sim O(u(0)^2)$ and $A_2\sim O(u(0)^2u_3(0))$ are constants depending on g and initial conditions. The cosine term in the above expression results in the observed dip of the total correlation function. The magnitude of the dip increases with increasing g.

The dynamical equation for the longitudinal component to $O(\epsilon)$ is likewise given by

$$\frac{\partial u_3^{(1)}}{\partial t}=(\nabla^2-2)u_3^{(1)}-[4u_+^{(0)}u_-^{(0)}+3(u_3^{(0)})^2] +2ig(u_+^{(0)}\nabla^2u_-^{(0)}-u_-^{(0)}\nabla^2u_+^{(0)}) -[4u_+^{(0)}u_-^{(0)}+(u_3^{(0)})^2]u_3^{(0)}. \tag{A6}$$

As before, the terms proportional to $(u_3^{(0)})^2$, the gradient terms and the cubic term are subdominant, and so the decay of the longitudinal correlation function $C_{\rm sm}^{\parallel}$ is given by

$$C_{\rm sm}^{\parallel}(\mathbf{r},t)=\langle\phi_3(\mathbf{x},t)\phi_3(\mathbf{x}+\mathbf{r},t)\rangle\sim\frac{B_1e^{-4t}}{t^{3/2}}\exp\left(-\frac{r^2}{8t}\right) -\frac{B_2e^{-2t}}{t^3}\exp\left(-\frac{r^2}{2t(3+g^2)}\right) +\frac{B_3}{t^{9/2}}\exp\left(-\frac{r^2}{4t(1+g^2)}\right), \tag{A7}$$

where $B_1\sim O(u_3(0)^2,u(0)^2)$, $B_2\sim O(u(0)^2u_3(0),u(0)^3)$, and $B_3\sim O(u(0)^4)$ are functions of g and initial conditions.

Note that $C_{\rm sm}^{\perp}$ evolves with a width that scales as $t^{1/2}$ and whose amplitude decreases as $t^{-3/2}$. The longitudinal $C_{\rm sm}^{\parallel}$ decays exponentially fast. This decay is consistent with our earlier assertion that the defects separated by a distance $L(t)$ hardly move over time scales corresponding to spin wave relaxation.

The cross correlator $C_{\rm scat}$ coming from the scattering of spin waves by moving defects, can be calculated by treating $\phi_{\rm sm}$ as ''slaved'' to $\phi_{\rm sing}$. As the defects move they excite spin waves, which decay in a time scale smaller than the time taken by the defects to move any further. The dominant contribution to $C_{\rm scat}$ comes from the product of Eq. (A3) and $\phi_{\rm sing}$. It is easy to see that this term leads to the same cosine dip as in Eq. (A5) but with an amplitude that decays algebraically in time. This is the source of the slow decay of the dip.

[1] A. J. Bray, Adv. Phys. **43**, 357 (1994).

[2] P. Chaikin and T. C. Lubensky, in *Principles of Condensed Matter Physics* (Clarendon Press, New York, 1994).

[3] K. Damle, S. N. Majumdar, and S. Sachdev, Phys. Rev. A **54**, 5037 (1996).

[4] G. F. Mazenko, Phys. Rev. B **42**, 4487 (1990); A. J. Bray and K. Humayun, J. Phys. A **25**, 2191 (1992).

[5] M. Seigert and M. Rao, Phys. Rev. Lett. **70**, 1956 (1993).

[6] A. J. Bray and S. Puri, Phys. Rev. Lett. **67**, 2670 (1991); H. Toyoki, *ibid.* **45**, 1965 (1992).

[7] In order to make such a claim, great care should be taken to avoid finite size effects. The tail of the autocorrelation function gets affected by the finite size of the lattice, earlier than the part of $C(r,t)$ used to calculate z. The decrease in the dip at $g=5$ can only be perceived when the system size is large.

[8] C. Yeung, M. Rao, and R. C. Desai, Phys. Rev. E **53**, 1 (1996).

[9] S. De Siena and M. Zannetti, Phys. Rev. E **50**, 2621 (1994).

[10] C. Yeung, A. Shinozaki, and Y. Oono, Phys. Rev. E **49**, 2693 (1994).

[11] H. K. Janssen, in *From Phase Transitions to Chaos*, edited by G. Györgyi *et al.* (World Scientific, Singapore, 1992).